

We are IntechOpen, the world's leading publisher of Open Access books Built by scientists, for scientists

6,000

Open access books available

148,000

International authors and editors

185M

Downloads

Our authors are among the

154

Countries delivered to

TOP 1%

most cited scientists

12.2%

Contributors from top 500 universities



WEB OF SCIENCE™

Selection of our books indexed in the Book Citation Index
in Web of Science™ Core Collection (BKCI)

Interested in publishing with us?
Contact book.department@intechopen.com

Numbers displayed above are based on latest data collected.
For more information visit www.intechopen.com



Chapter

The Effects of Blade Configurations on Performance of a Tidal Vertical Axis Turbine

Sepideh Amiri Tavasoli, Seyed Jalal Hemmati, Saeed Niazi and Ali Jalali

Abstract

Hydrokinetic energy contains the major uncontrolled source of renewable marine energy. The highest level of converter technology readiness offered in the last three decades is TRL8–9, which is related to the first-generation horizontal axis converters. In low-depth calm waters, one of the best options to harvest tidal energy is vertical axis turbines. About 16% of the conceptual designs presented in the last 30 years apply this type of converter, which does not have a high level of technological readiness. In this study, a laboratory-designed vertical axis turbine has been introduced in which the effects of the number of blades, the blade profile, and attack angle on the performance of the turbine were analyzed. A 3D incompressible viscous turbulent computational finite volume approach is applied, with the spatial second-order and temporal first-order accuracies. The turbulent model $k-\omega$ SST was used to obtain the flow inside the turbine. Rotors include two, three, and six blades with three different profiles, including NACA2421, NACA16021, and NACA0020. Computational results reveal that the turbine with three blades and an angle of attack of $+8^\circ$ using the NACA2421 profile has a maximum generation capacity of about 4 kW, with a strength factor of 0.4 and a power factor of about 20%. The capacity, however, was lower for a higher number of blades.

Keywords: renewable tidal energy, in-stream tidal turbine, CFD, vertical axis turbine

1. Introduction

Tidal energy technology is a cluster of four technologies, namely tidal dams, tidal lagoons, tidal current converters (TISECs), and dynamic tidal power (DTP) that use tidal cycles to generate electricity [1]. The greatest unrestrained potential of tidal energy is from the tidal current source. This unlimited source of clean energy can be estimated with high accuracy and reliability. Practically, to extract the tidal energy, the average flow velocity in the spring tide of neighborhoods should be faster than 1.5–2.5 m/s. Nevertheless, in nearly 10 regions in the world, the flow velocity is relatively high.

Zeiner-Gundersen [2] proposed a simple and cost-effective vertical axis turbine with flexible foils designed based on inspiration from hydrodynamic thrust

characteristics of aquatic creatures. These novel aspects resulted in a high-performance turbine that attained up to a 0.37 power coefficient in a confined channel and could self-start at low inflow water velocities.

Pongduang et al. [3] studied the helical tidal current turbine and reported its performance and characteristics, aiming to develop the free water flow electric turbine. The scaled model of the tidal turbine was built as 0.5 and 0.6 m in diameters and 1.25 m in length. The turbine cross-section blade was symmetric NACA0020 with a 0.07 m chord length and three blades with the helical angle of 120°, 135°, and 150°. The model was tested in a towing tank.

Priegue and Stoesser [4] investigated the influence of blade roughness on the performance of a vertical axis tidal turbine. In this design, the vertical axis of turbines undergoes stall at some periods, that is, the flow separates from the blade during each revolution. In this study, it is hypothesized that roughening turbine blades causes a delay of the flow separation (similar to flows over rough bluff bodies), which in turn diminishes the turbine stall, and ultimately results in an increase in the performance of the turbine.

Based on an experimental study, Harries et al. [5] analyzed the performance and optimization of a prototype novel drag-driven vertical axis a tidal stream turbine. Hamidi et al. [6] also investigated the power and momentum coefficients of a three-blade vertical tidal turbine using a laboratory model. Bouzaher et al. [7] investigated a vertical axis tidal turbine with flexible blades, with the focus on analyzing the effect of flexible airfoil types and the blade flexibility on the net output power of the turbine. Delafin et al. [8] used the variable pitch in order to control the angle of the attack of blades continuously during their rotation. The same approach is also considered in this study. Based on the 2D blade-resolved unsteady Reynolds-Averaged Navier-Stokes (RANS) simulations, the improvement caused by pitching the blades is evaluated in a three-straight-blade vertical axis tidal turbine. Three pitching laws are defined and tested, aiming to reduce the angle of the attack of the blades in the upstream half of the turbine, but no pitching motion in the downstream half.

Airfoil is a geometric structure to generate mechanical force from the relative motion between the airfoil and the airflow around the airfoil structures. The first wind turbine blades were also designed by airfoils used in aviation applications. However, in the 1980s, due to defects in aeronautical airfoils applied to a wind turbine, special air airfoils were assigned to wind turbines. A wind turbine has been created with the help of special airfoils. The airfoil series for controlled wind turbines, with variable level adjustment by stations, was developed by the National Renewable Energy Laboratory in 1984 [9].

Vertical axis turbines and their hydrodynamic performances have not been well investigated. This type of turbine is very suitable for calm and shallow water conditions, which are very common around the world. In this study, the flow in a microturbine under calm and shallow water conditions is examined based on a simulation. Using the hybrid mesh and finite volume approach simulation methods, the effects of the number and profile and angles of the attack of turbine blades on the performance of vertical axis turbines are studied.

2. Numerical method

The governing equations to solve the 3D incompressible flow are the time-averaged continuity equation and the time-averaged momentum equations:

$$\frac{\partial \bar{u}}{\partial x} + \frac{\partial \bar{v}}{\partial y} + \frac{\partial \bar{w}}{\partial z} = 0 \quad (1)$$

$$\frac{\rho D \vec{v}}{Dt} = \rho \vec{g} - \nabla \vec{p} + \nabla \cdot \vec{\tau} + \vec{f} \quad (2)$$

where \vec{g} is the force of gravity, \vec{f} is the volumetric force, and $\vec{\tau}$ is the stress tensor, which is presented as follows:

$$\vec{\tau} = (\mu + n) \left(\frac{\partial \bar{u}_i}{\partial x_j} + \frac{\partial \bar{u}_j}{\partial x_i} \right) \quad (3)$$

In Eq. (3), both the viscous shear stress and the turbulent or eddy shear stress are included. The time average method is used to simulate turbulence effects. In these models, new terms are introduced to simulate turbulence of the mean flow instead of explicitly examining the turbulence behavior. These are the time-averaged Navier-Stokes equations that are applied for a larger-scale modeling of turbulence problems.

Turbulent modeling is relatively difficult because it requires detailed information about the structure of the turbulence phenomenon in the fluid, which is often not available. Therefore, one of the available turbulence models can be used to determine the magnitude of the stresses. In this study, the $k-\omega$ SST¹ model is used as the turbulence model. The $k-\omega$ SST model is based on two equations, which is actually a combination of two models—standard $k-\omega$ and $k-\varepsilon$. The $k-\omega$ SST model effectively uses the high precision of the standard $k-\omega$ formulation near walls, as well as the independence of the $k-\varepsilon$ model, and for this reason, it has gotten rid of the problem of the $k-\omega$ standard model, which is highly sensitive to the turbulent properties of the input current. For this reason, the $k-\omega$ SST model has better performance than both $k-\varepsilon$ and $k-\omega$ models.

The operational performance of marine turbines can be defined as dimensionless coefficients. These coefficients are the tip speed ratio (TSR), thrust coefficient (C_T), and power coefficient (C_p):

$$\text{TSR} = \frac{\omega R}{V} \quad (4)$$

$$C_T = \frac{T}{\frac{1}{2} \rho V^2 A} \quad (5)$$

$$C_p = \text{TSR} \times C_T \quad (6)$$

where ω is the rotational speed of the turbine, R is the radius of the blade, V is the inlet axial flow velocity, A is the hypothetical surface of the turbine disk, and T denotes the turbine thrust [10]. One of the most important variables, which indicates the effect of the number of blades, is the solidity ratio:

$$\sigma = \frac{NC}{\pi D} \quad (7)$$

where N is the number of blades and C is the length of their airfoil chord.

¹ Shear stress transport.

In this chapter, a 3D laboratory-designed vertical turbine is modeled, and a finite volume method is used to simulate the hydrodynamic performance of the turbine. The length of the airfoil chord is 120 mm, the spiral angle (the angle between the blade and the horizontal plate) is 60° , the height and the diameter of the turbine are both 300 mm, and the number of blades is two, three, and six (**Figure 1**). Among the available options, profiles of the NACA2421, NACA0020, and NACA16021 are chosen. **Figure 2** illustrates the cross-sectional shape of each of the three selected profiles.

The outer part of the model is considered similar to that used by Revuz et al. [11]. As shown in **Figure 3**, the computational domain has a length of 4500 mm, width of 3000 mm, and height of 1500 mm, which includes a rotating part with a diameter of 400 mm and a height of 320 mm. The diameter of the internal section is 200 mm and its height is 320 mm.

Figures 4–6 show grids, the turbine blade, and total solution domain meshes, respectively. As mentioned before, the moving mesh was employed, and the adjacent areas to the object have smaller mesh size than the other areas. The mesh sensitivity analysis was also performed; the results of which are presented in **Figure 7**. Optimally, the number of computational cells was about 3.5 million. The Ansys fluent software is used. A high-performance (HP) server with five nodes, each with the ability to connect to 56 clients and 256 Gbyte ram, and a total of 5 terabyte hard disk space were used. Each performance took between 2 and 8 days.

Simulations are performed for different TSRs and the results are compared. A complete cycle of sea tides lasts for 14 days, during which every 6 hours, the



Figure 1.
3D model of a rotor designed with three blades.

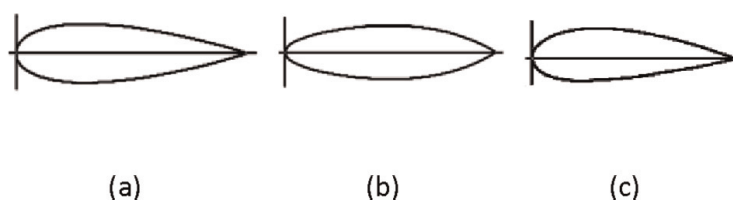


Figure 2.
A top view of the blade section with profiles of (a) NACA0020, (b) NACA16021, and (c) NACA2421.

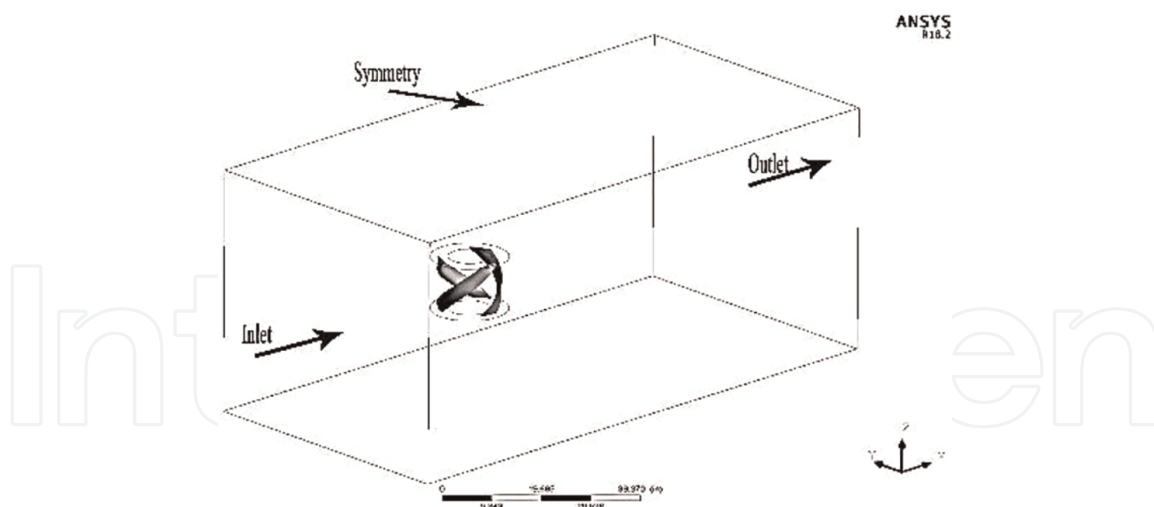


Figure 3.
Computational domain of the simulation of the hydrodynamic turbine.

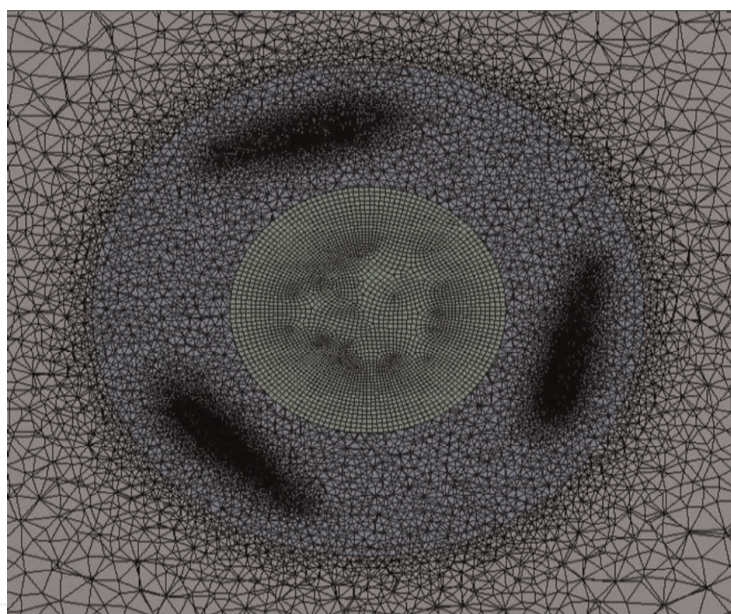


Figure 4.
Internal computational grids.

horizontal velocity of the current rises to the maximum from zero, and then falls back to zero. **Figure 8** depicts an example of speed series on the Qeshm channel in the Persian Gulf [12].

Laboratory results reported by Talukdar et al. [13] were used to validate our results. In their study, the water flow velocity was 0.87 m/s, and the density of seawater was 1.025 kg/m^3 . Torque coefficients and computational power obtained in our study are compared against the laboratory data present in a study by Talukdar et al. [13] and presented in **Figures 8** and **9**. As can be seen, for the NACA0020 type, the profiles are similar in both studies. A comparison of analytical and experimental results reveals that the maximum relative error for the torque coefficient and the computational power coefficient was 18% and 20% less than the experimental values, respectively. The way the generator is connected to the blade, as well as uncertainties in experimental data, contributed to some errors, but changes in torque and power coefficients in different TSRs were similar in both cases.

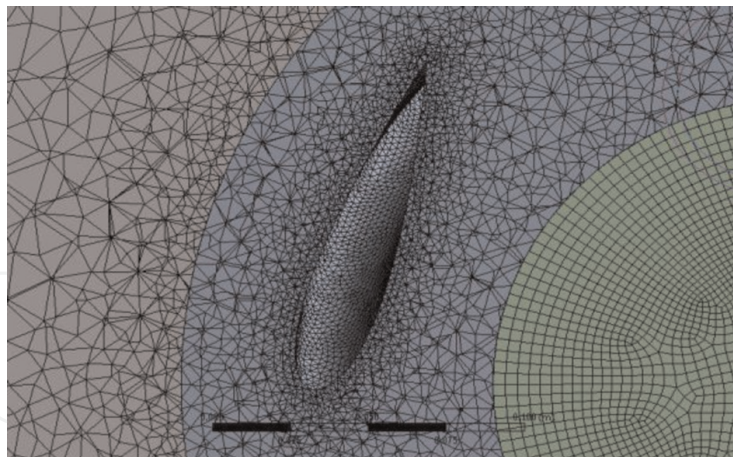


Figure 5.
Grids of the turbine blade.

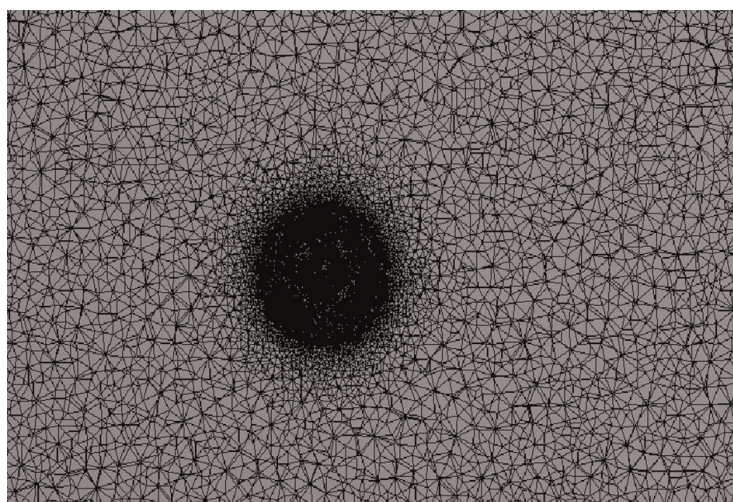


Figure 6.
Total solution of the domain mesh.

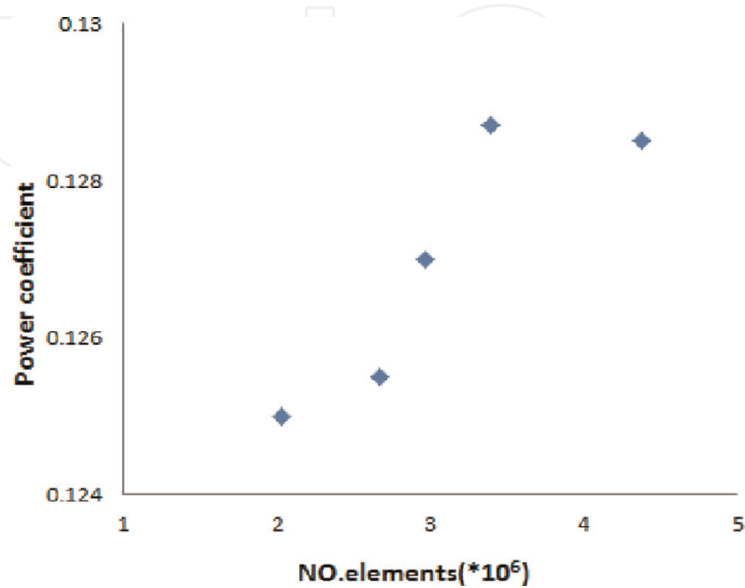


Figure 7.
The grid sensitivity analysis.

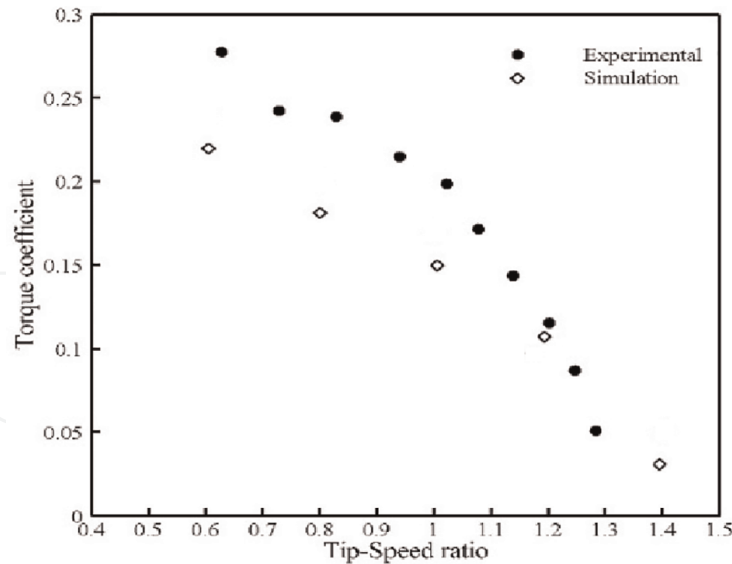


Figure 8.
Comparison of torque coefficient for different TSRs with experimental data [13].

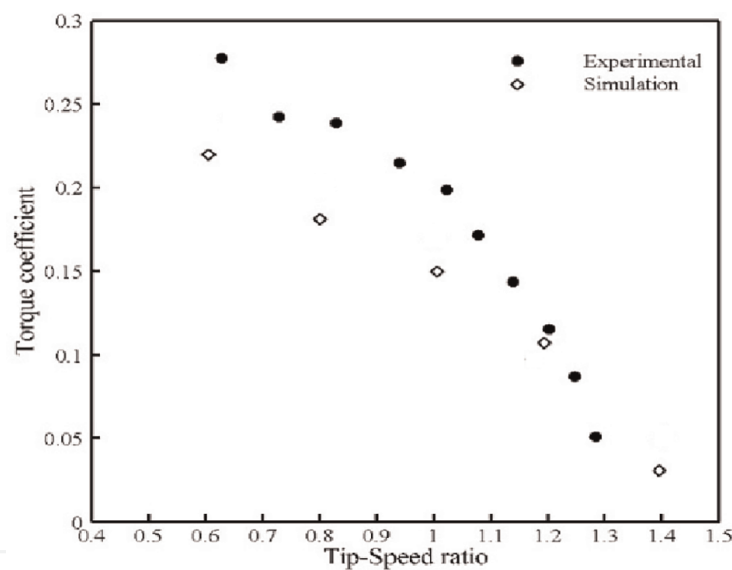


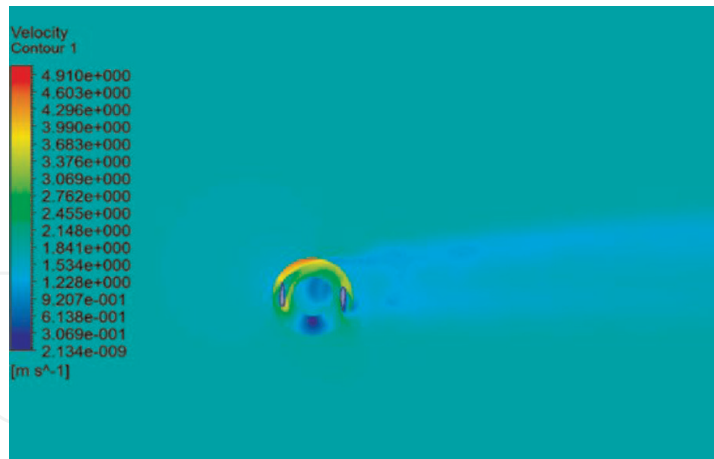
Figure 9.
Comparison of power factor for different TSRs with experimental data [13].

3. Results and discussion

Figures 10–16 depict simulated velocity and pressure and the velocity vector around the blades for different blade numbers and profiles. Only results of the simulations under the maximum velocity (1.8 m/s) are shown. In these figures, it is assumed that the stream enters horizontally from the left side at a constant mean speed and exits from the right side.

Figure 10 shows that the maximum flow velocity inside the turbine when collides with blades is 3.7 m/s for turbines with two blades. This value is 3.6 and 2.8 m/s for turbines with three and six blades, respectively. The most turbulent flow is behind the turbine with six blades, as illustrated in Figure 10c.

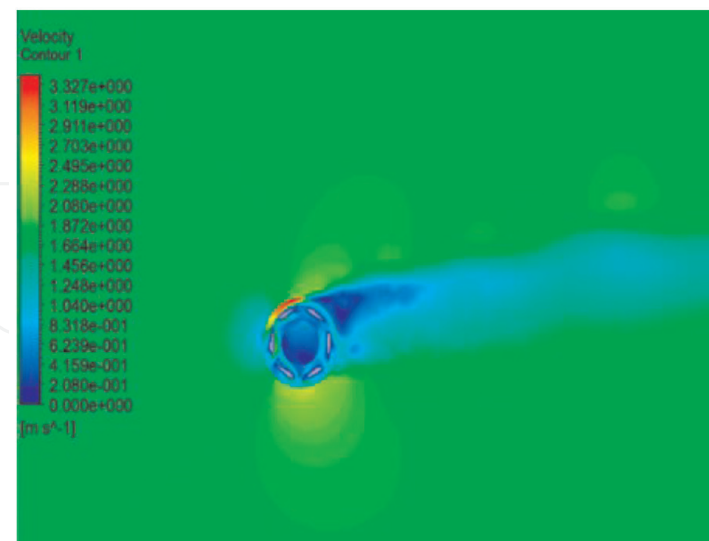
Analysis of the velocity distributions for the turbines with different blade numbers indicates that the current deviation in the increasing order is for the two-, three-, and,



(a)



(b)

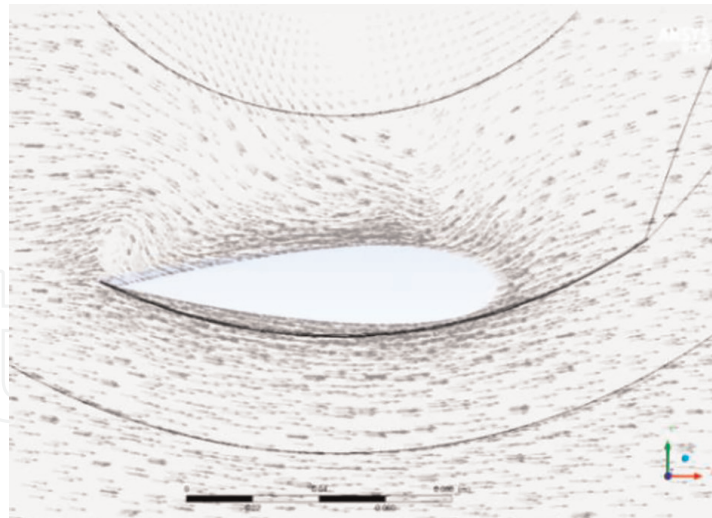


(c)

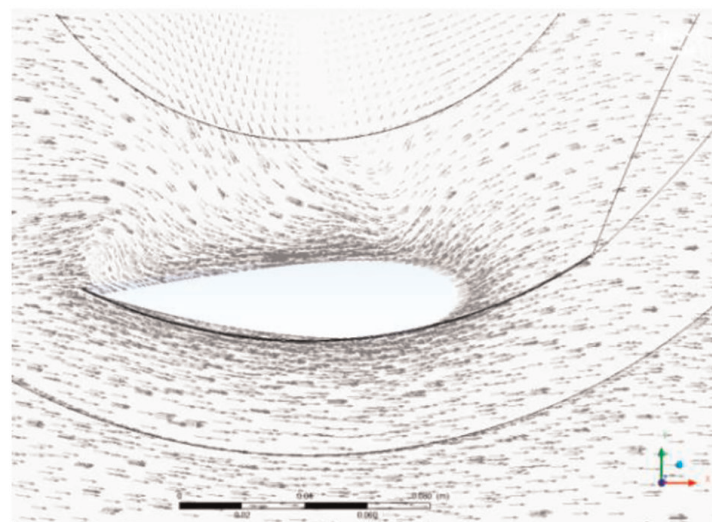
Figure 10.

A top view of the velocity contour for (a) two-blade, (b) three-blade, and (c) six-blade turbines with a speed of 1.8 m.

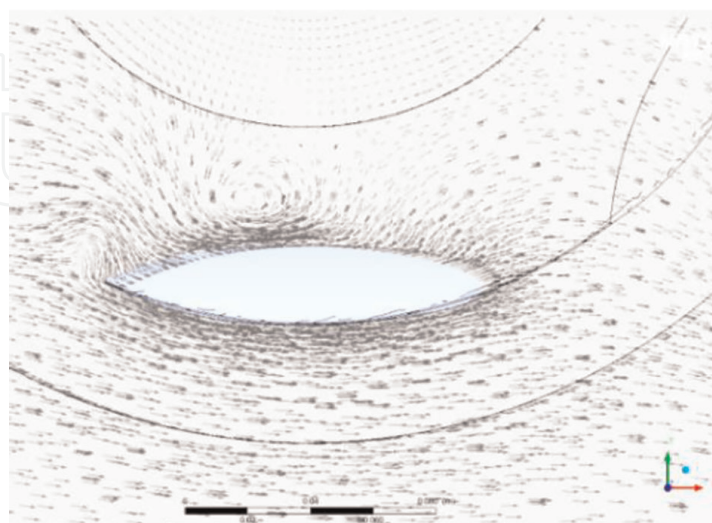
six-blade turbines, respectively (**Figure 10**). If the turbine has a large flow deviation, more energy should be consumed. Thus, the smaller the flow deviation, the better the turbine in terms of energy production. From the edge of the attack to the tail of the



(a)



(b)



(c)

Figure 11.
Speed vector around the blade for the input speed of 1.8 m/s in the profile mode of (a) NACA16021, (b) NACA2421, and (c) NACA16021.

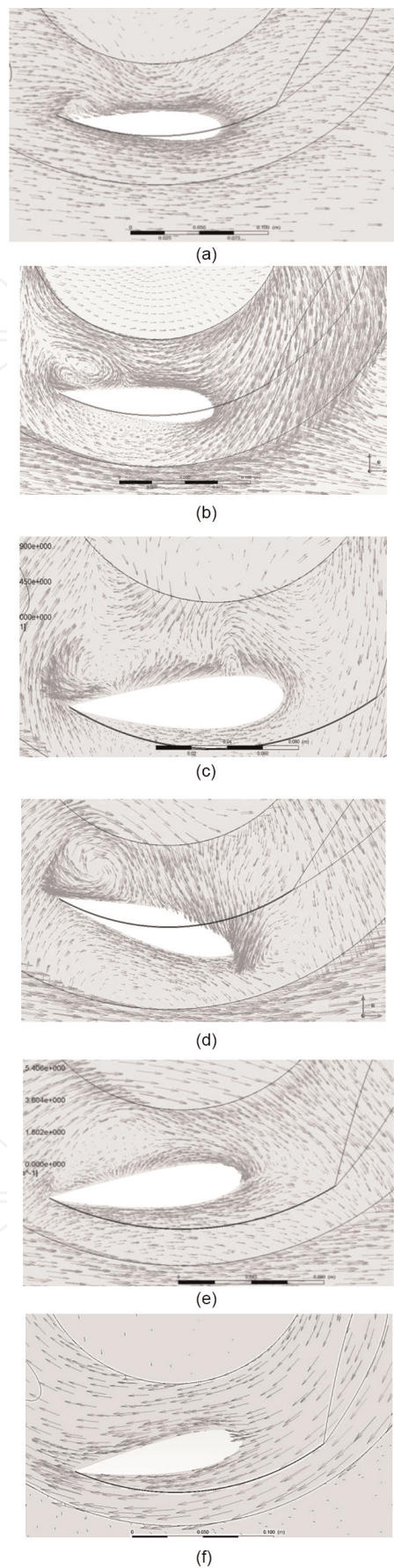


Figure 12. Speed vector around a blade for the input speed of 1.8 m/s in the angle of the attack mode (a) The angle of $+4^\circ$ (b) The angle of $+8^\circ$ (c) The angle of $+12^\circ$ (d) The angle of 0° (e) The angle of -8° (f) The angle of -12° .

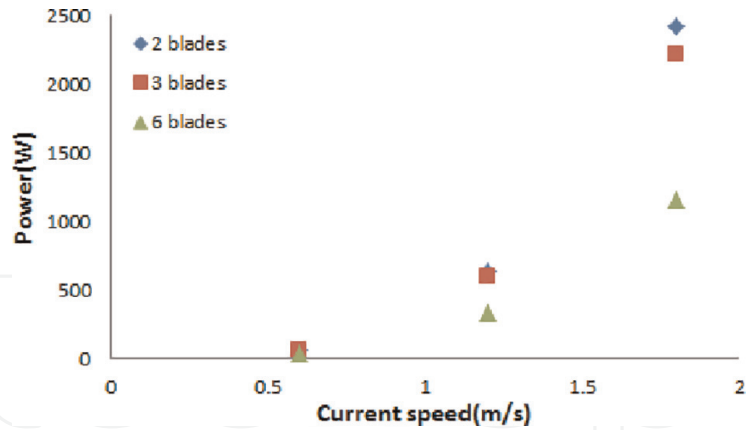


Figure 13.
 Tidal energy versus stream velocity for different blade numbers.

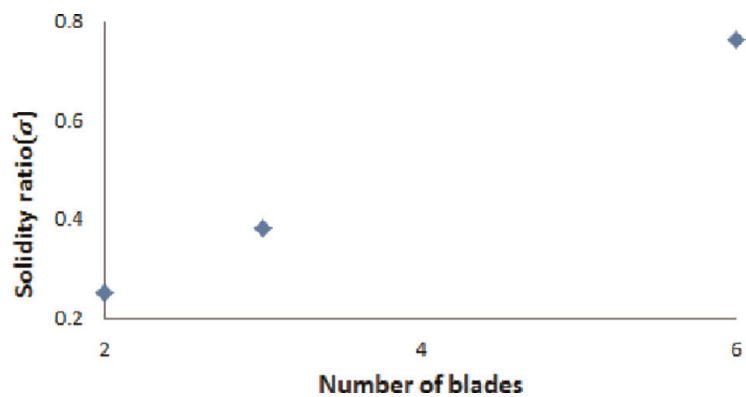


Figure 14.
 The solidity coefficient for different number of blades.

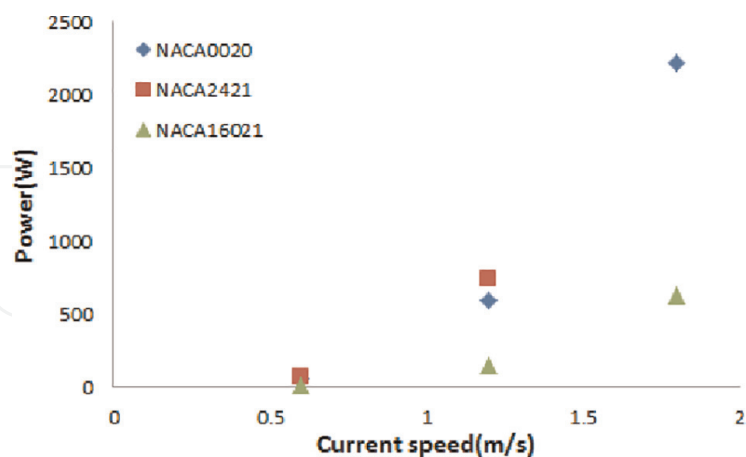


Figure 15.
 Tidal energy versus stream velocity for different blade profiles.

airfoil, pressure initially decreases but then begins to increase, and the increase in pressure leads to the separation of the boundary layer, which increases the pressure gradient and may cause problems in the turbine blades.

Figure 11 shows the velocity distribution for turbines with different blade profiles, but the inlet maximum speed of 1.8 m/s. Flow deviation in the turbine with the NACA2421 profile is less than the others, causing the extraction of more energy from

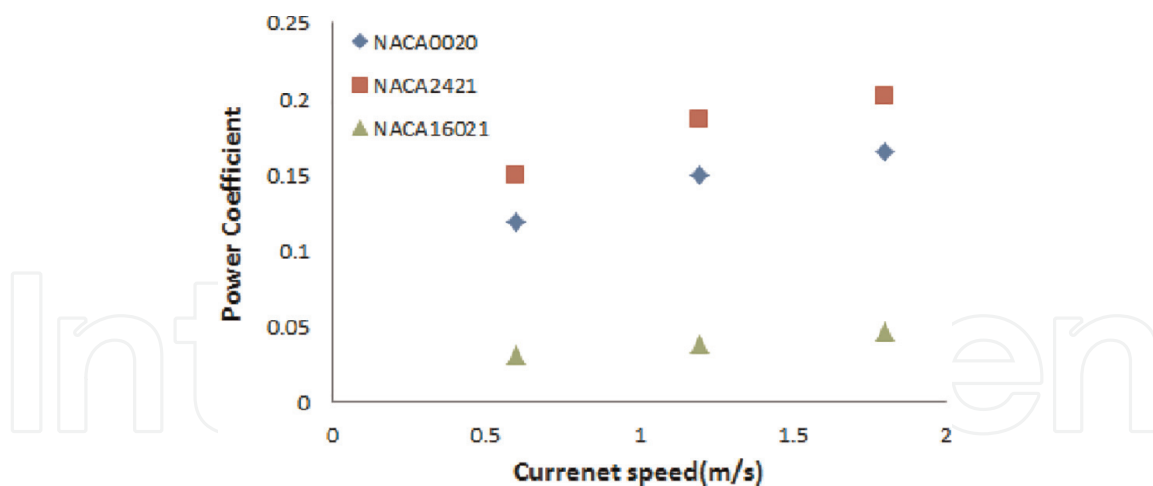


Figure 16.
Power coefficient versus stream speed for different blade profiles.

the tidal water. **Figure 11** also shows that the vorticity value in the turbine with the NACA2421 profile is less than the other two types, which improves the performance of the turbine.

As a turbine with the NACA2421 profile is the most optimal at the flow velocity of 1.8 m/s, it was designed and shaped under different angles.

One of the issues that always complicates the simulation of vertical axis turbines is the continuous interaction of the fluid with blades in each section of the rotor. In fact, a fluid that is affected by a blade in the upstream area should hit the blades in the lower half of the rotor.

In general, by reducing the angle of the attack of both negative and positive angles at upstream, some current separation occurs at the end of the airfoil, which causes a severe pressure difference at the upper and lower levels of the airfoil (**Figure 12**), which leads to an increase in the return time of the current from turbulence to laminar. This pressure difference, along with the destructive phenomenon of dynamic fatigue and the circular currents of the airfoil tip, leads to the destructive drag force. In response to this force, the speed may be reduced and some severe vibrations may be created in the turbine. If this condition continues to increase, the pressure on the blade structure can have far more dangerous effects, such as breaking the blades. These vortices will be increased in the negative angles as far as the reverse pressure is observed. There is also increased in positive angles with increasing the angle of these vortices. At an angle of $+8^\circ$, which is in line with the flow direction, the end of the blade is covered with vortices, but at an angle of $+4^\circ$, it can be seen that in addition to the end of the blade, vortices are formed on the curvature of the blade.

Figure 13 presents the amount of tidal energy obtainable for different velocities of flow for turbines with two, three, and six blades. As the speed increases, the output power increases, but the increase in the two-blade mode is greater than that of three or six blades. This result can also be seen in **Figure 10**. In general, with increasing the number of blades, the speed of the rotor rotation decreases, but torque increases. Similarly, as the number of blades increases, the solidity of the turbine increases (**Figure 14**). As in the case of a three-blade turbine, the solidity factor is more than two blades and the power that can be produced does not decrease considerably when the number of blades increases, the pressure distribution decreases. Thus, the fatigue stress with oscillating loads created in turbines with fewer blades causes the blades to break and damage. The two-blade turbine produces more energy than a three-blade

turbine, but because of the high pressure on its blades, it causes the turbine to sag. Naturally, this loosening motion causes stability problems for the turbine. It also increased stress on the components of the turbine, such that they may break down over time. The two-blade turbine generally causes environmental problems due to issues such as loss of components and the need for repair and also increases the maintenance costs of the turbine. However, the amount of power produced in a three-blade turbine is not that much different from that in a two-blade turbine. The cost of a three-blade turbine is also lower, and it leads to less environmental impact. On the other hand, when blades are more than three, there is more water resistance and the power generation is slower. Thus, a three-blade turbine is more efficient. For these reasons, a three-blade turbine is ideal because of its high-energy performance, greater stability, and durability. As a result, a three-blade turbine is selected as the most optimal turbine in terms of the blade number.

Airfoil is a geometrically shaped structure for mechanical force generation from the relative movement between the airfoil and the surrounding airflow of the airfoil structures [14]. For wind turbines, the airfoil shape of the blades influences the turbine power production. The lifting efficiency of blades determines the effectiveness of rotor rotation for the productive energy conversion from wind kinetics to rotor rotation, which leads to higher electricity generation from the drive unit.

The boundary layer of the airfoil is exerted by additional pressure generated by the curvature shape of the airfoil compared to the constant pressure on the boundary layer made of the plate with zero incidences. The pressure distribution on the edge of the boundary layer is the same as the pressure distribution on the wall in the plate. However, due to the streamline curvature of the airfoil surface, pressure gradients and compensation for the centrifugal force of the streamline flow are generated inside the boundary layer. Furthermore, the transition point of the boundary layer on the airfoil is determined by the outer flow and its pressure difference generated by the curvature shape of the surface [15].

As each profile is from different NACA series, there are some differences. In the NACA0020, the thickness of the profile was 20%, while in the NACA2421 and NACA16021, it was 21%.

As can be seen in **Figure 15**, the NACA2421, which is thicker than the NACA0020 and is more curved than both the NACA0020 and NACA16021, produced more energy. On the other hand, the NACA0020, which is less thick than the NACA16021, produced more energy. As a result, the amount of energy production decreases with increasing the thickness and increases with increasing the curvature. As a result, the most optimal type of profile among the studied profiles is the NACA2421, which is a four-digit and asymmetric NACA series. Thus, this profile is selected as the optimal profile.

As expected, power generation by different profiles increases when the speed increases, but for the NACA2421 profile, this increase is the most. Hence, in the maximum current velocity of 1.8 m/s, it is predicted that a power of 2.5 kW can be obtained.

Figure 16 shows the tidal energy in terms of stream velocity in turbines with different profiles. A turbine with three blades (NACA2421) generates the highest power at different speeds, with a maximum of 20%.

Figures 17 and **18** show the coefficient of power and extractable power relative to the ratio of different tip velocities for different attack angles, and **Figures 19** and **20** show the extractable power and power factor relative to different attack angles for different velocity ratios.

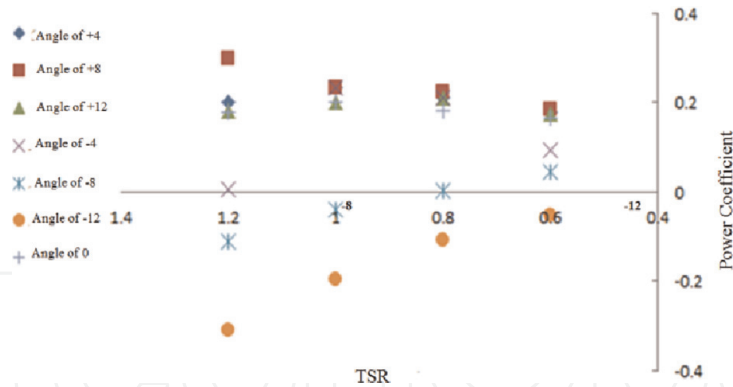


Figure 17.
Power factor diagram of the tip speed ratio for different attack angles.

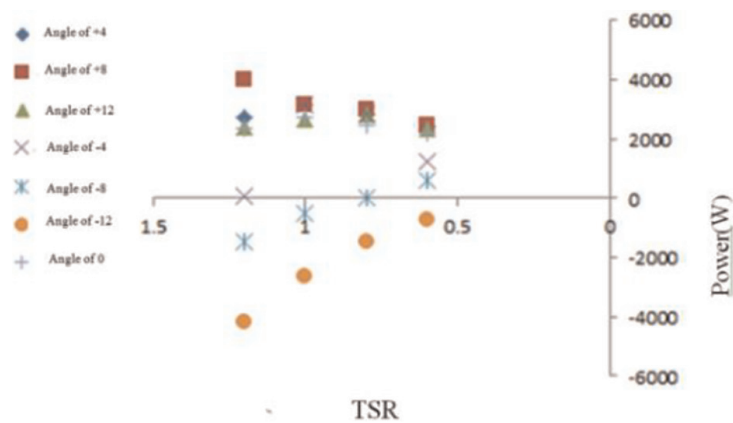


Figure 18.
Power diagram based on the tip speed ratio for different attack angles.

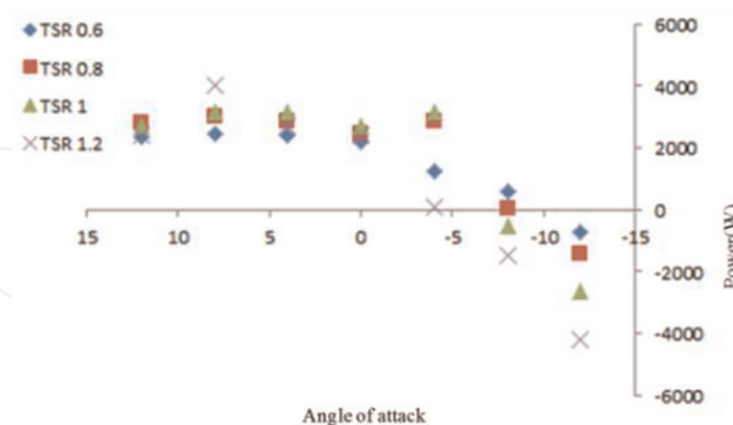


Figure 19.
Power diagram of different attack angles for the tip speed ratio.

As shown in **Figures 17–20**, the turbine has the highest power factor at a certain tip speed ratio, which is the optimal tip speed ratio, and changes power depending on the blade angle of the attack. The optimal tip velocity ratio changes with the angle of the attack relative to the reference mode, so that the maximum increase is at the angle of the attack of $+8^\circ$. At negative angles, it first increases at the angle of the attack of -4° , but then it decreases. As the airfoil angle of the attack increases, the power factor decreases over time.

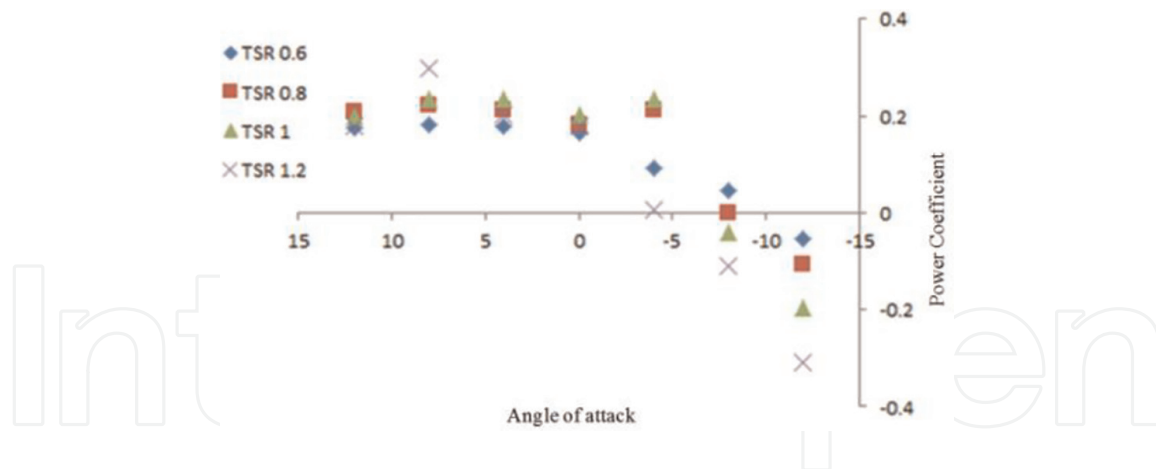


Figure 20.
Power factor diagram of different attack angles for the tip speed ratio.

According to these diagrams, it can be seen that the optimum power output of the turbine in terms of the attack angle is a turbine with an attack angle of +8, which produces a power of about 4000 watts, about 1.5 times more than the power that can be produced by a turbine with the zero-degree angle of the attack. Nevertheless, the pressure on the turbine blades increases by 7% in the turbine with the optimum power output compared to that with the zero-degree angle of the attack, although this increase in pressure is negligible.

4. Conclusion

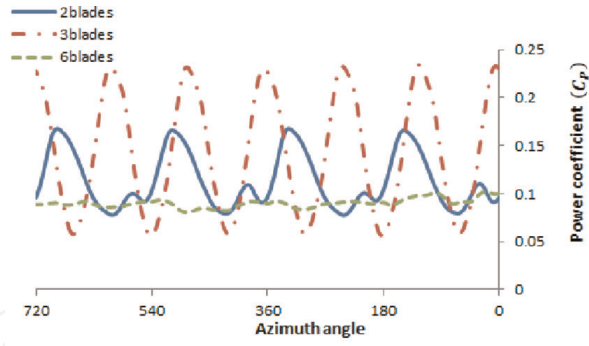
Figure 21 shows the power factor in two turbine rotation cycles for different speed ratios. It can be seen that for different tip speed coefficients, the amount of power extracted from the three-blade turbine was the most. With increasing the speed of the tip, the amount of power further increased, but decreased for three-blade and two-blade turbines, respectively.

According to **Figure 22**, at different blade tip speeds, the power factor in a turbine with the NACA2421 blade profile is higher than a turbine with the NACA0020 profile. According to **Figure 22**, the optimal tip velocity ratio is equal to TSR1 because it has the highest output power factor.

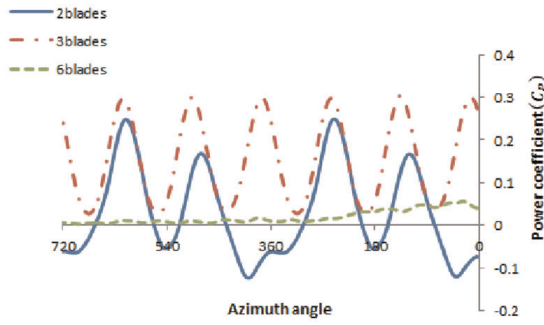
According to **Figure 23**, the power factor has changed for angles of 0 and +8°, with the maximum value in TSR 1.2 for the angle of +8°. Increasing the angle of the attack from 0 to +8° increases the power factor, but at the angle of +12, it decreases. The maximum power belongs to the turbine with the attack angle of +8° and the tip speed ratio of 1.2 (**Figure 24**).

Our analysis showed that an increase in the number of blades negatively affects the obtainable power. In other words, the solidity coefficient increases with increasing the number of blades. This increase has destructive environmental impacts, including the noise generated by the blades, as well as the pollution during construction, transmission, and installation of the blades [16]. As a result, according to the simulations, the turbine axis with three blades yields better performance.

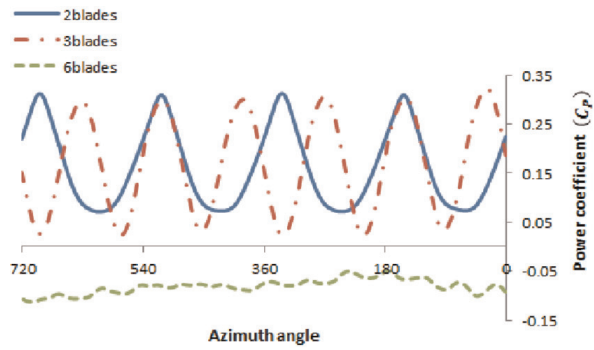
The simulation results also predict that the curvature and thickness of the blade profile affect the production capacity. The production capacity is directly related to the increase in the curvature of the blade profile and is inversely related to its



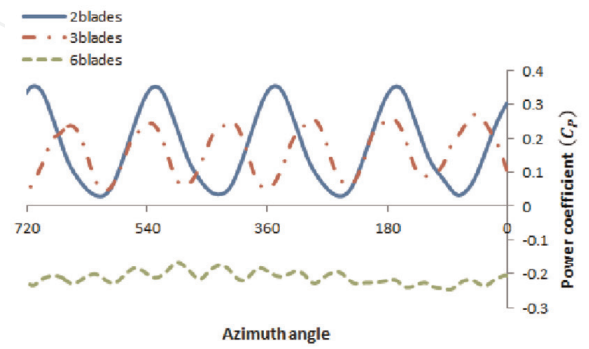
(a)



(b)

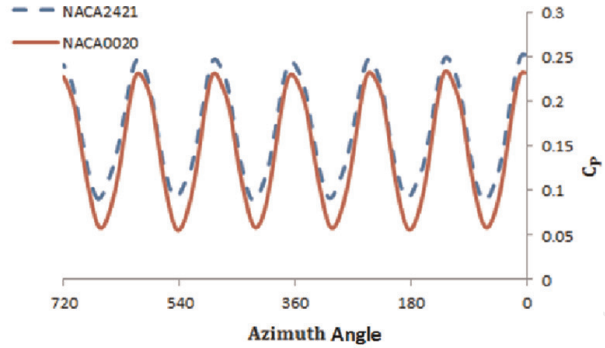


(c)

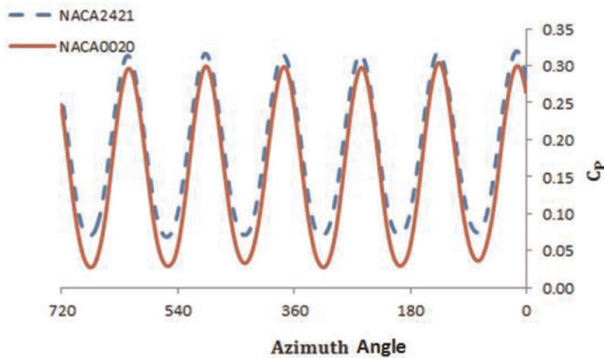


(d)

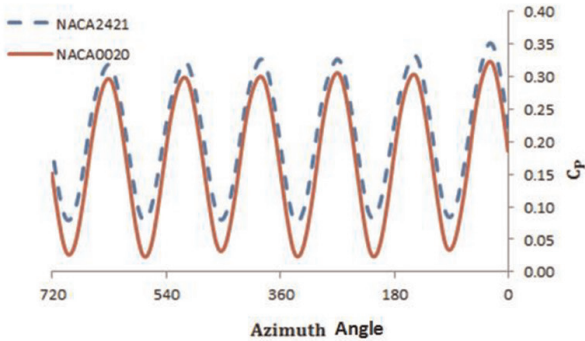
Figure 21. Comparison of power factor diagram of a torsion angle at different tip speed ratios for a turbine with two, three, and six blades. (a) TSR 0.6, (b) TSR 0.8 (c) TSR 1 (d) TSR 1.2.



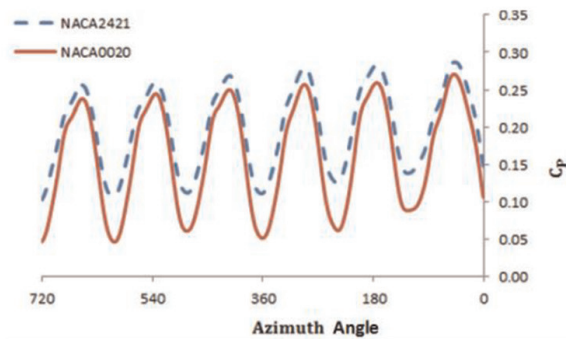
(a)



(b)



(c)



(d)

Figure 22. Comparison of power factor diagrams in two turbine revolutions for the NACA0020 and NACA2421 profiles at different tip speeds. (a) TSR 0.6, (b) TSR 0.8 (c) TSR 1 (d) TSR 1.2.

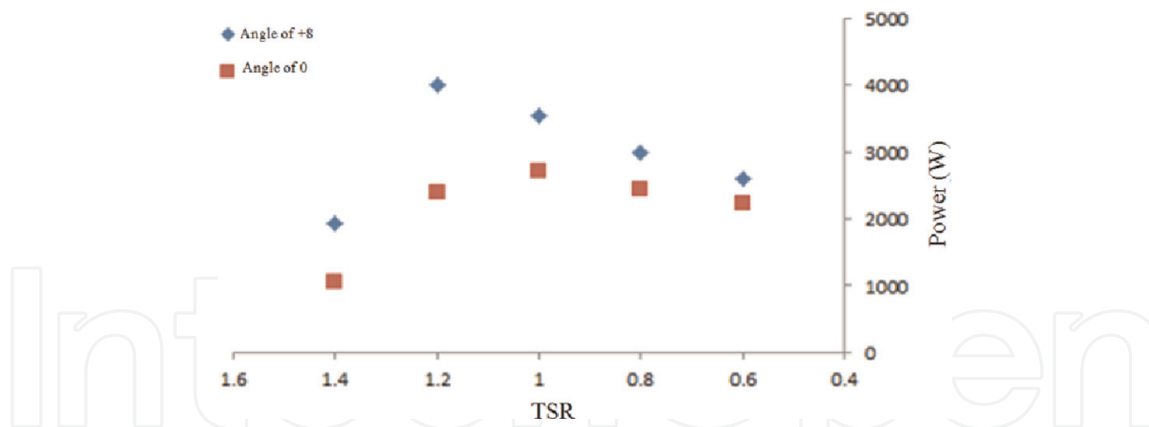


Figure 23. Comparison of the power graphs of the tip velocity ratios for attack angles of 0 and +8°.

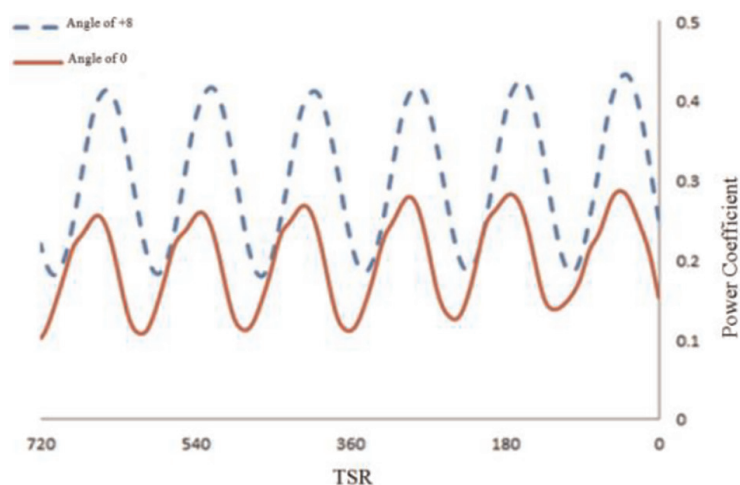


Figure 24. Comparison of power factor diagrams in two turbine revolutions for the angle of +8° and 0° in TSR1.2.

thickness. The production capacity in this study was estimated to be 4 Kw for a three-blade turbine and the NACA2421 profile.

Although in experimental tests [13], the experimental power has been reported to be higher than the computational value in the current research, trend changes in design indicators and the amount of existing error are acceptable. This method can be used to design suitable microturbines at the entrance of bays, shrimp ponds, and in the water outlet of boilers.

Acknowledgements

This research was carried out with the support of the Electricity Company of Hormozgan province, Iran, as a “plan to measure the production of electricity from marine energy in Hormozgan region in the Persian Gulf.” The authors appreciate and thank the esteemed management and members of the company’s research committee.

IntechOpen

Author details


Sepideh Amiri Tavasoli¹, Seyed Jalal Hemmati^{1*}, Saeed Niazi¹ and Ali Jalali²

1 Faculty of Engineering, University of Hormozgan, Department of Mechanical Engineering, Bandar Abbas, Iran

2 Department of Mechanical Engineering, Mashhad Payam Noor University, Mashhad, Iran

*Address all correspondence to: hemmati@hormozgan.ac.ir

IntechOpen

© 2022 The Author(s). Licensee IntechOpen. This chapter is distributed under the terms of the Creative Commons Attribution License (<http://creativecommons.org/licenses/by/3.0>), which permits unrestricted use, distribution, and reproduction in any medium, provided the original work is properly cited. 

References

- [1] Magagna D, Uihlein A. JRC Ocean Energy Status Report: Technology, Market and Economic Aspects of Ocean Energy in Europe. European Union, 2015; 2014
- [2] Zeiner-Gundersen DH. A novel flexible foil vertical axis turbine for river, ocean, and tidal applications. *Applied Energy*. 2015;**151**:60-66
- [3] Pongduang S, Kayankannavee CH, Tiaple Y. Experimental investigation of helical tidal turbine characteristics with different twists. *Energy Procedia*. 2015, 2015;**79**:409-414
- [4] Priegue L, Stoesser TH. The influence roughness on the performance of a vertical axis tidal turbine. *International Journal of Marine Energy*. 2017;**17**: 136-146
- [5] Harries T, Kwan A, Brammer J, Falconer R. Physical testing of performance characteristics of a novel drag-driven vertical axis tidal stream turbine; with comparisons to a conventional Savonius. *International Journal of Marine Energy*. 2016;**14**:215-228
- [6] Hamidi R. CFD Simulation of Experimental Vertical Axis Tidal Turbine in Persian Gulf Region. 2019
- [7] Bouzaher MT, Guerira B, Hadid M. Performance Analysis of a Vertical Axis Tidal Turbine with Flexible Blades. 2017. DOI: 10.1007/s11804-017-1391-0
- [8] Delafin P, Deniset F, Astolfi J, Hauville A. Performance improvement of a Darrieus Tidal turbine with active variable pitch. *Energies*. 2021;**14**:667
- [9] Tangler JL, Somers DM. NREL airfoil families for HAWT's. In: *Wind Power*. Washington; 1995. pp. 117-123
- [10] Shamsi R, Ghasemi H. Hydrodynamic performance analysis of horizontal marine current turbines using computational fluid dynamics. In: 15th Conference on Marine Industries, MIC2013 (in Persian). 2013
- [11] Revuz J, Hargreaves DM, Owen JS. On the domain size for the steady-state CFD modeling of a tall building. *Wind and Structures*. 2012;**15**(4):313-329
- [12] Monitoring and Modeling Studies of Iranian Coasts. Ports and Maritime Organization, Private Communication; 2019
- [13] Talukdar PK, Kulkarni V, Saha UK. Field-testing of model helical bladed hydrokinetic turbines for small scale power generation. *Renewable Energy Journal*. 2018
- [14] Manwell J, McGowan F, Rogers JG, A. L. *Wind Energy Explained: Theory, Design and Application*. 2nd ed. UK: Wiley; 2009. p. 704
- [15] Schlichting H, Gersten K. *Boundary-Layer Theory*. Berlin, Heidelberg: Springer; 2017. p. 805
- [16] Mohammadi A, Farahat S, Mohammadi M, Mohammadi MR. Investigating the effect of using different airfoils in Output power of horizontal axis wind turbine blade. In: *Fourth International Conference on New Approaches to Maintenance Energy*